International Journal of Concrete Structures and Materials
Vol.9, No.3, pp.283–294, September 2015
DOI 10.1007/s40069-015-0111-x
ISSN 1976-0485 / eISSN 2234-1315

Heavy Metal Leaching, CO_2 Uptake and Mechanical Characteristics of Carbonated Porous Concrete with Alkali-Activated Slag and Bottom Ash

G. M. Kim, J. G. Jang, Faizan Naeem, and H. K. Lee*

(Received July 9, 2015, Accepted August 17, 2015, Published online September 1, 2015)

Abstract: In the present study, a porous concrete with alkali activated slag (AAS) and coal bottom ash was developed and the effect of carbonation on the physical property, microstructural characteristic, and heavy metal leaching behavior of the porous concrete were investigated. Independent variables, such as the type of the alkali activator and binder, the amount of paste, and CO_2 concentration, were considered. The experimental test results showed that the measured void ratio and compressive strength of the carbonated porous concrete exceeded minimum level stated in ACI 522 for general porous concrete. A new quantitative TG analysis for evaluating CO_2 uptake in AAS was proposed, and the result showed that the CO_2 uptake in AAS paste was approximately twice as high as that in OPC paste. The leached concentrations of heavy metals from carbonated porous concrete were below the relevant environmental criteria.

Keywords: porous concrete, coal bottom ash, alkali activated slag, carbonation, heavy metal leaching.

1. Introduction

Porous concrete is defined as a type of concrete with continuous open voids (Sriravindrarajah et al. 2012). In general, porous concrete is fabricated with a uniform size of coarse aggregates without fine aggregates to create continuous voids into concrete intentionally (Sriravindrarajah et al. 2012). Since the development of porous concrete in Japan in the 1980s, it has been applied in various ways to restore groundwater supplies and to reduce the runoff from a site (Sriravindrarajah et al. 2012; Bhutta et al. 2012). In recent years, industrial by-products such as coal ash and slag have attracted several studies to utilize the materials in the fabrication of eco-friendly porous concretes (Jang et al. 2015a; Park and Tia 2004).

Since the voids in porous concrete are mainly formed by coarse aggregates, a morphological characteristic of the aggregate is deemed most important, and need to be of uniform size, rough surface, and low specific gravity (Jang et al. 2015a). Coal bottom ash (BA) is generated by the combustion of pulverized coal, and many features of BA largely satisfy the aforementioned conditions to fabricate a porous concrete (Singh and Siddique 2014; Kim et al. 2014a). In particular, the highly porous structure and the rough surface property of BA is suitable for forming sufficient voids in the matrix of porous concrete (Kuo et al. 2013; Kim et al. 2014b). However, BA contains and may leach a variety of heavy metals such as cadmium, copper, and lead, inhibiting a broad range of applications in a construction industry (Jang et al. 2015a).

Several attempts have been made to immobilize the heavy metals in a cementitious matrix. Li et al. reported that a cement based matrix could be effective to immobilize Cu, Pb, and Zn (Li et al. 2012). Such heavy metals could be encapsulated in the calcium silicate hydrate (C–S–H) phase of a Portland cement matrix (Li et al. 2012). Zhang et al. found that fly ash based geopolymer can immobilize Cr(VI), Cd(II), and Pb(II), relying on the chemical binding and precipitation of the heavy metals (Zhang et al. 2008). Alkali-activated slag (AAS) paste is also known as an effective material to immobilize heavy metals. Deja found that AAS paste can immobilize Cd, Zn and Pb up to 99.9 % (Deja 2002).

In order to fabricate a porous concrete, AAS paste using blast furnace slag (BFS) was considered in the present study. The immobilization effectiveness of AAS paste has been reported in several studies, and details can be found in Shi and Fernandez-Jimenez (2006), Qian et al. (2003a, 2003b). However, the microstructure and pH in AAS paste could be significantly affected by the carbonation process (Kar et al. 2014). In particular, pH in carbonated AAS paste can be decreased to 9 or lower, and the solubility of some heavy metals may be increased (Puertas et al. 2006; Bernal et al. 2014). Thus, the effect of carbonation on the leaching characteristics of heavy metals in porous concrete should be investigated.

In addition to immobilization of heavy metals, AAS paste can be used for uptake of CO_2 which is a typical greenhouse

Department of Civil and Environmental Engineering, Korea Advanced Institute of Science and Technology, Daejeon 305-701, South Korea.
*Corresponding Author; E-mail: haengki@kaist.ac.kr

gas. In most studies on carbonation of AAS paste, calcium carbonate was only considered as a carbonated product (Park and Tia 2004; Kim et al. 2013; Deja 2002). Eloneva et al. reported that AAS paste can be used for CO_2 uptake via the carbonation of calcium components (Eloneva et al. 2008). However, sodium carbonates in previous studies were found in AAS paste when NaOH or water glass was used as an alkali activator (Puertas et al. 2006; Bernal et al. 2014), thus the sodium carbonates should be considered to evaluate the CO_2 uptake of AAS paste (Bertos et al. 2004).

In the present study, a porous concrete with alkali activated slag and coal bottom ash was developed. BFS and BA were used as a binder and an aggregate material, respectively, for the fabrication of the porous concrete. Since carbonation is known to induce not only the change in physicochemical properties of AAS but also the change in the leaching behavior of heavy metal from BA, the present study aims to investigate the effect of carbonation on heavy metal leaching, mechanical property and CO_2 uptake of porous concrete through a series of characterization tests. Independent variables, such as the type of the alkali activator and binder, the amount of paste, and CO_2 concentration, were considered.

2. Experimental Program

2.1 Materials

The chemical compositions of BFS and BA used in this study, are listed in Table 1. The BA was obtained from the Seo-Cheon thermoelectric power plant, sieved in the range of 2.5–5.0 mm, and was then washed to remove impurities from the surface. The absolute volume ratio of the BA to design the mixing proportion was calculated in accordance with the procedure described in JIS A 1104 (2006), and the result was approximately 39 %. Inductively coupled plasma (ICP, iCPA-6300 Duo ICP-OES and ICP/MS 7700X) spectrometers were used to measure the total amount of heavy metals in the BA, and the results are listed in Table 2. Detailed test procedures for the ICP analysis of BA can be found in Jang et al. (2015a).

Sodium hydroxide (NaOH), and a mixture of water glass and sodium hydroxide were used as alkali activators. The sodium hydroxide with the specific gravity of 2.13 was used in the form of pellets. The chemical composition of the waterglass produced by Duksan Chemicals Co. Ltd., was SiO_2 of 28–38 wt% and Na_2O of 9–19 wt%, and its specific gravity was 1.38.

2.2 Mix Proportion and Fabrication Process of Porous Concrete

The mix proportion of the porous concretes is listed in Table 3. Three different types of porous concretes were fabricated in this study. The AAS-based porous concretes were categorized according to the type of alkali activator, and were compared with the OPC-based porous concretes. The effect of alkali activator on the AAS-based porous concretes was investigated by using two different types of alkali activator, i.e., one sodium hydroxide and both sodium hydroxide and waterglass. It has been reported in many studies that silicate modulus (Ms: SiO_2/Na_2O) of 1.0–1.5 and Na_2O to slag ratio of 4 % were appropriate to ensure an appropriate compressive strength of AAS paste (Wang and Scrivener 1995). Therefore, in the present study, the silicate modulus was chosen to be 1.2 and controlled by an addition of sodium hydroxide and water (Ravikumar and Neithalath 2013; Chi et al. 2012). The Na_2O/slag was fixed at 4 % for all the alkali activators. The liquid to binder ratio of AAS-based porous concretes and the water to cement ratio of OPC-based porous concretes were fixed at 0.5 and 0.3, respectively. Paste to aggregate (P/G) ratios were varied from 25 to 35 % to investigate the effect of P/Gs on the physical properties of porous concrete. The P/G of PC2 was kept identical to that of NS2 and SS2, i.e., 30 %, to examine the effect of the binder type on the properties of the porous concrete.

The specimens were cast into the cylindrical molds with a diameter of 10 cm and a height of 20 cm. The mixing procedure was as follows: BA and BFS were mixed for 1 min and alkali activator was then added to the dry mixture. Then, mixing was conducted for further 3 min. Since the compaction process can significantly affect the mechanical properties of porous concretes, the process was carefully controlled as follows: Half of the mold was filled with the mixture, and a tamping bar was used to compact the mixture 10 times. Then, the rest of the mold was fully filled, and a vibrator was used to compact the mixture for 10 s. The specimens were demolded after 2 days and cured for 28 days. The specimens were cured under temperature of 25 ± 5 °C and ambient humidity in laboratory condition.

The mix proportion of the paste specimens is shown in Table 4. The same mixing proportion as the part of paste for

Table 1 Chemical compositions of BFS, OPC and BA.

Chemical composition (%)	Blast-furnace slag (BFS)	Ordinary Portland cement (OPC)	Coal bottom ash (BA)
CaO	56.10	65.9	3.95
SiO_2	21.00	10.6	50.10
Al_2O_3	17.00	3.8	26.90
Fe_2O_3	0.62	3.89	10.80
SO_3	0.77	2.26	–

Table 2 Measured heavy metal contents of BA by ICP analysis (in ppm).

Cr	As	Cu	Cd	Hg	Pb
121.952	3.416	276.220	139.524	ND[a]	355.578

[a] ND: non detected.

Table 3 Mix proportion of porous concretes (unit: kg/m^3).

Series	Binder material	BA	Water	NaOH	Waterglass	W/B	P/G (%)
NS1	248.1	662.3	110.9	13.1	–	0.5	25
NS2	285.6	636.8	127.7	15.1	–	0.5	30
NS3	319.6	613.7	142.9	16.9	–	0.5	35
SS1	259.5	661.7	79.2	8.4	42.2	0.5	25
SS2	297.6	637.0	90.9	9.6	48.4	0.5	30
SS3	333.5	613.6	101.8	10.8	54.2	0.5	35
PC2	365.0	642.4	109.5	–	–	0.3	30

P/G: ratio of paste by the weight of aggregates. NS: porous concrete fabricated with slag and NaOH (Na_2O/Slag: 4 %). SS: porous concrete fabricated with slag, waterglass and NaOH (Na_2O/Slag: 4 %, silicate modulus (Ms): 1.2). PC2: porous concrete fabricated with Portland cement and water.

Table 4 Mix proportion of paste specimens.

Series	Binder material	water	NaOH	Waterglass	W/B
NS(P*)	6.37	2.85	0.336	–	0.5
SS(P)	6.67	2.03	0.215	1.083	0.5
PC(P)	9.66	2.90	–	–	0.3

*P: paste specimen.

porous concrete was adopted to fabricate pastes in an effort to investigate the carbonation effect on the microstructure. The size of these specimens was 50 mm × 50 mm × 50 mm, and the curing condition was identical to that of the porous concretes.

2.3 Experimental Details

2.3.1 Accelerated Carbonation Test

An accelerated carbonation test was conducted on the porous concretes and pastes at a temperature of 20 °C and a relative humidity of 65 %. All specimens were exposed to a CO_2 concentration of 5 or 10 % in a carbonation chamber for 2 weeks. Non-carbonated specimens were prepared as references in a sealed condition to prevent natural carbonation. The carbonated specimens were cut at the center, and a phenolphthalein spraying test was performed on the cut surface of the specimens to measure the carbonation depth.

2.3.2 Microstructural Analysis of AAS Pastes

A mercury intrusion porosimetry (MIP) test was conducted on the pastes, using a porosimeter (Auto pore IV 9500, Micromeritics Instrument Corporation). The pressure in the test increased up to 414 MPa to detect a pore diameter in the range of 0.003–1000 μm (Ravikumar and Neithalath 2013). The surface tension and the contact angle in the experiment were set at 0.485 N/m and 130°, respectively (Ravikumar and Neithalath 2013). A thermogravimetric/differential thermal analysis (TG/DTA) was performed to analyze the hydration and carbonation products in the pastes. The heat rate and the flux of nitrogen gas in the test were set at 30 °C min and 100 ml min, respectively (Kim et al. 2013; Ravikumar and Neithalath 2013). The temperature was varied from 30 to 1000 °C (Kim et al. 2013).

2.3.3 Void Ratio Test

The open-void ratio (V_{open}) and closed-void ratio (V_{close}) of the porous concretes were calculated with Eqs. (1) and (2), respectively (Jang et al. 2015a; Kim and Lee 2010).

$$V_{open} = \left(1 - \frac{(W_2 - W_1)\rho_w}{V_1}\right) \times 100\,\% \tag{1}$$

$$V_{close} = \left(1 - \frac{(W_3 - W_1)\rho_w}{V_1}\right) \times 100\,\% - V_{open} \tag{2}$$

Here, W_1 is the weight of the specimen submerged in water, W_2 is the weight of the specimen dried in air for 24 h, W_3 is the weight of the specimen dried in an oven, V_1 is the volume of the specimens, and ρ_w is the density of water (Jang et al. 2015a; Kim and Lee 2010). The total void ratio (V_{total}) was calculated as the sum of V_{open} and V_{close} (Jang et al. 2015a; Kim and Lee 2010).

2.3.4 Compressive Strength Test

Compressive strength tests of the porous concretes were conducted in accordance with the procedure described in ASTM C39 (American Society for Testing and Materials 2012). The top and bottom surfaces of each specimen were ground to prevent any concentrated loading. The specimens were tested at an age of 28 days using a 3000 kN universal testing machine (UTM). A displacement control method was adopted, and the speed of the cross-head of the UTM was held at 0.01 mm/s.

2.3.5 Heavy Metal Leaching Test

A leaching test on the porous concretes was conducted to analyze the leaching behavior of the heavy metals in accordance with the NSF/ANSI 61-2007a (2007) (Drinking water system components-Health effects) (NSF International standard/American National Standard, NSF/ANSI 61-2007a 2007). The test solution of leaching test was changed after first, second and fourth day, and the solution was collected on each day. The pH of the solution, at a level of 4–5, was adjusted with nitric acid, and ICP-MS was used to measure the leached concentrations of the heavy metals from the testing solution including chromium, arsenic, copper, lead, mercury, and cadmium. In previous studies, toxicity characteristic leaching procedure (TCLP) method has been adopted to characterize the leaching behavior of heavy metals (e.g., Dermatas and Meng 2003; Perera et al. 2005). TCLP method requires the sample to be equal or greater than 3.1 cm^2/g or smaller than 1 cm in its narrowest dimension, otherwise it necessitates crushing, cutting or grinding of the specimen (Environment, Health and Safety Online 2008). Since the porous concrete does not fit into the size specified in TCLP method, grinding of the porous concrete is mandatory that could expose the BA covered by the AAS paste. In contrast, since the NSF/ANSI 61-2007a does not specify the dimension of a sample for the test procedure, the original form of the porous concrete can be maintained in the course of the test (NSF International standard/American National Standard, NSF/ANSI 61-2007a 2007).

3. Results and Discussion

3.1 Carbonation Behavior of AAS Pastes

The measured carbonation depths of AAS and OPC pastes after exposure to CO_2 are shown in Fig. 1 and summarized in Table 5. The extent of the carbonation in the OPC paste (PC(P)_C5) at a 5 % CO_2 concentration was slight, and the carbonation depth was no greater than 3 mm at all sides. In contrast, the AAS pastes underwent deeper and more intense carbonation than OPC paste did. The carbonation depth of AAS pastes at a 5 % CO_2 concentration varied according to the type of the alkali activator. The carbonation depth in the AAS paste incorporating the waterglass-based alkali activator (SS(P)_C5 specimen) was slightly lower than that of the AAS paste using NaOH (NS(P)_C5 specimen).

The total porosity and the average pore diameter of the pastes are shown in Table 6. The average pore diameter of the non-carbonated AAS pastes (NS(P)_C0 and SS(P)_C0) specimens varied according to the type of alkali activator. SS(P)_C0 specimen showed a smaller average pore diameter than NS(P)_C0 specimen. Such differences in the average pore diameters according to the type of the alkali activator presumably affected the carbonation rate (see Table 5), since high porosity can cause an increase in the diffusivity of CO_2 (Bertos et al. 2004). In the phenolphthalein spraying test, the high porosity of NS(P)_C5 could cause deeper carbonation depth than SS(P)_C5 specimen.

NS(P)_C0 and SS(P)_C0 specimens showed lower porosity in comparison with PC(P)_C0 specimen. After exposure to accelerated carbonation, the porosity of NS(P)_C10 and SS(P)_C10 specimens increased, whereas that of PC(P)_C10 specimen decreased. In general, OPC paste is known to have more calcium components in the residues of C_3S, C_2S, and $Ca(OH)_2$ in the pore solution than AAS paste (Bakharev et al. 2001). This condition may act as a buffer for the decalcification of C–S–H phases in the OPC paste (Bakharev et al. 2001). In addition, the carbonated products in an OPC matrix can create a protective area that can interfere with the diffusion of CO_2, filling the pores with the carbonated products (Bernal et al. 2014; Ylmén and Jäglid 2013). Thus, the formation of carbonates under the rich calcium condition can reduce the porosity of an OPC matrix (Bernal et al. 2014; Bakharev et al. 2001). In contrast, AAS paste has lower buffer in the pore solution such as $Ca(OH)_2$ and calcium components than OPC paste (Bernal et al. 2014; Bakharev et al. 2001). Hence, the carbonation of AAS pastes in the test was mainly caused by the decalcification from C–S–H phases, leading to an increase in the porosity (Bakharev et al. 2001).

The pore size distribution of the pastes is summarized in Table 7. The percentage of pores in the range of 0.1–10 μm increased slightly in PC(P)_C10 sample after carbonation, while the percentage of pores in the range of 0.01–0.1 μm declined slightly. In NS(P)_C10 and SS(P)_C10 samples, the percentage of pores in the range of 0.1–100 μm increased after carbonation, while the percentage of pores in the range of 0.01–0.1 μm decreased. In particular, the percentage of pores in NS(P)_C10 and SS(P)_C10 samples ranging from 0.1 to 1.0 μm significantly increased. It can be inferred from the results that the decalcification of C–S–H phases in AAS pastes induced a change in the percentage of pores ranging from 0.1 to 1.0 μm.

Figure 2 shows the TG/DTA curves of the paste samples. The weight loss of C–S–H phases and carbonated products in the TG/DTA curves is summarized in Table 8. The weight loss from 50 to 200 °C was used as an indicator of the interlayer water weight of the C–S–H phases (Kim et al. 2013). Before carbonation, the weight loss of NS(P)_C0 and SS(P)_C0 samples in the temperature range was much higher than that of PC(P)_C0 sample. After carbonation, the weight loss of the C–S–H phase in SS(P)_C10 and NS(P)_C10 samples decreased by more than 30 % compared to SS(P)_C0 and NS(P)_C0 samples, whereas the reduction in the weight loss of PC(P)_C10 was slight compared to PC(P)_C0. These results can support that

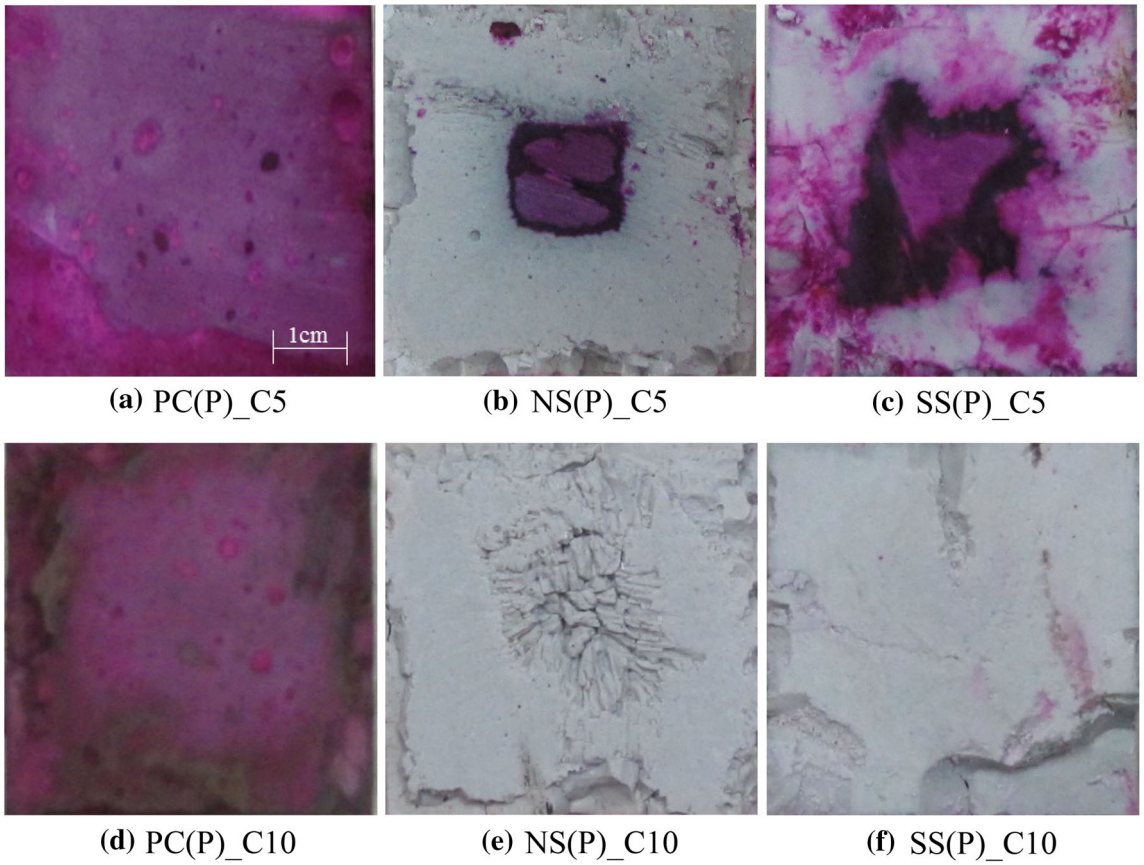

Fig. 1 Carbonation depth of AAS and OPC pastes according to CO_2 concentration: C5 and C10 indicate 5 and 10 % CO_2 concentration, respectively.

Table 5 Measured carbonation depth of paste specimens.

Specimen	PC(P)_C5*	PC(P)_C10	NS(P)_C5	NS(P)_C10	SS(P)C5	SS(P)_C10
Carbonation depth (mm)	3.33	5.33	17.67	25	14.33	25

Table 6 Total porosity and average pore diameter of paste specimens.

Specimen	PC(P)_C0	PC(P)_C10	NS(P)_C0	NS(P)_C10	SS(P)_C0	SS(P)_C10
Total porosity (%)	19.59	14.12	21.54	22.90	18.20	20.56
Average pore diameter (μm)	0.0270	0.0207	0.0167	0.0152	0.0103	0.0105

Table 7 Pore size distribution (PSD) of paste specimens.

PSD (%)	Pore diameter (μm)					
	>100	100–10	10–1.0	1.0–0.1	0.1–0.01	<0.01
PC(P)_C0	0.9	6.4	4.8	10.3	68.0	12.2
PC(P)_C10	1.1	2.1	7.9	16.1	58.1	17.4
NS(P)_C0	1.4	3.8	2.2	1.8	73.6	17.4
NS(P)_C10	0.6	7.2	4.0	27.5	29.9	31.1
SS(P)_C0	1.2	3.2	1.6	1.3	47.2	45.9
SS(P)_C10	0.8	7.6	8.3	10.8	32.3	43.0

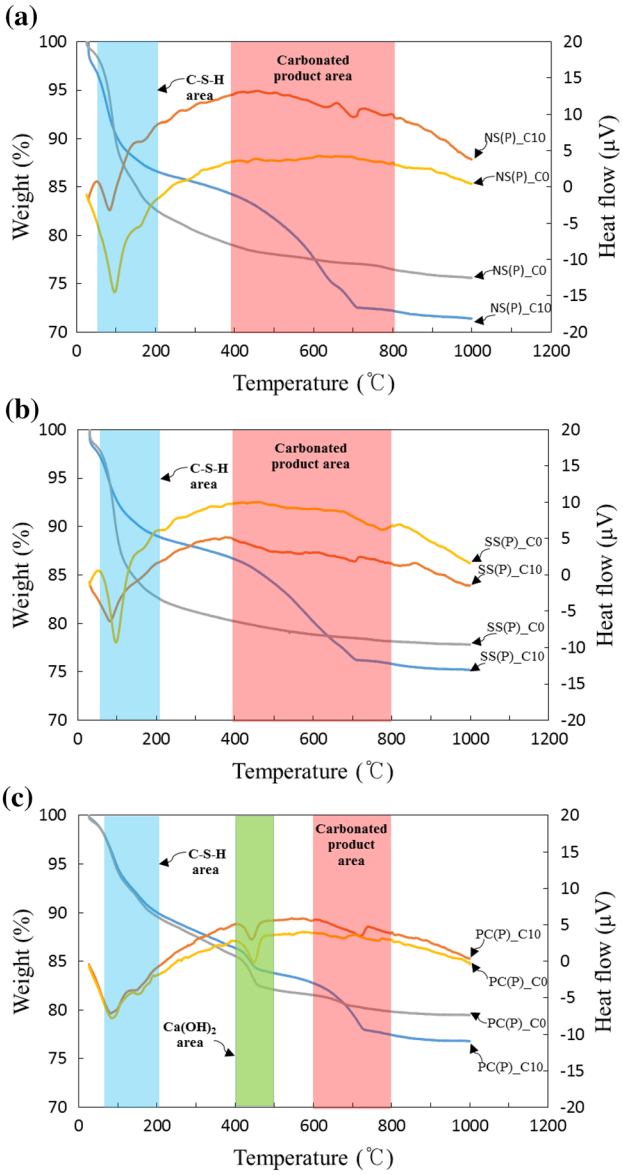

Fig. 2 TG/DTA test results of AAS and OPC pastes: **a** AAS pastes with NaOH (NS(P)), **b** AAS pastes with waterglass (SS(P)) and **c** OPC pastes (PC(P)).

carbonation of the AAS pastes in the present study was mainly caused by the decalcification from the C–S–H phases (Bernal et al. 2014; Bakharev et al. 2001).

The decomposition temperature of calcium carbonates such as calcite and vaterite was defined at the peak range of 600–800 °C in many studies (Kim et al. 2013). In the present study, the weight loss of SS(P)_C10 and NS(P)_C10 samples in the temperature range was similar to that of PC(P)_10 sample, whereas the carbonation depth of SS(P)_C10 and NS(P)_C10 specimens was much deeper than that of PC(P)_C10 specimen. This may be due that BFS has a relatively low calcium content compared to Portland cement (Puertas et al. 2006; Bakharev et al. 2001) and the aqueous concentration of calcium leached from the AAS pastes becomes low under a highly alkaline condition (Song and Jennings 1999). In addition, porosity of AAS paste increases as carbonation progressed. That is, relatively small amount of calcium component in AAS paste can form calcium carbonates and an increase in porosity due to carbonation can improve the diffusivity of CO_2 under those conditions. Consequently, the carbonation depth of AAS paste can be deeper than that of OPC paste, while the weight loss indicating calcium carbonates between them can be similar.

In the present study, an amended temperature range of carbonated products was proposed in an effort to accurately evaluate the uptake of CO_2 in AAS pastes. In general, calcium carbonates are mainly considered as a carbonated product in AAS pastes. However, sodium carbonates such as natron or trona can also exist in AAS pastes, when using a sodium incorporated alkali activator (Puertas et al. 2006; Bernal et al. 2014). Natron is a compound with sodium decahydrate ($Na_2CO_3{\cdot}10H_2O$) and sodium bicarbonate ($NaHCO_3$), and more than 80 % of natron consists of sodium decahydrate (Edwards et al. 2007). The release of CO_2 from the sodium decahydrate initiates at a temperature of 400 °C, exhibiting an endothermic reaction (Guo et al. 2011). Since trona loses water at the temperature below 100 °C and forms sodium carbonate, a similar reaction could

Table 8 Weight loss of C–S–H and carbonated products in the TG/DTA curves.

Phases	Temperature range (°C)	Weight loss (%)					
		PC(P)_C0	NS(P)_C0	SS(P)_C0	PC(P)_C10	NS(P)_C10	SS(P)_C10
C–S–H	50–200	9.27	15.90	15.44	8.90	10.26	8.61
Calcium carbonates (calcite, vaterite)	600–800	1.67	1.00	0.72	5.31	5.49	4.35
Calcium carbonates (calcite, vaterite) & sodium carbonates (natron, trona)	400–800	1.67	2.40	2.08	5.31	11.95	10.79

also begin at 400 °C (Ekmekyapar et al. 1996; Jang et al. 2015b). The downward slope of the DTA curves of SS(P)_C10 and NS(P)_C10 samples indicated an occurrence of the endothermic reaction that was observed at 400 °C (see Fig. 2a, b), and a dramatic change in the weight loss in the TG curve was initiated at 400 °C, simultaneously. This temperature is the identical point that the release of CO_2 from sodium carbonates is initiated (Guo et al. 2011; Ekmekyapar et al. 1996). Thus, it seems that the temperature range of 400–800 °C in the TG/DTA curves is more suited to define the uptake of CO_2 in AAS pastes.

In PC(P)_C10 sample, the TG/DTA curves within the proposed temperature range also showed a trend similar to that of SS(P)_C10 and NS(P)_C10 samples. However, it is well known that the weight loss and the trend of the DTA curve in PC(P)_C10 sample is caused by the decomposition of $Ca(OH)_2$ (Kim et al. 2013). That is, the weight loss within the proposed temperature range in PC(P)_C10 sample indicated the decomposition of $Ca(OH)_2$. In contrast, $Ca(OH)_2$ is not exist in AAS paste (Shi and Fernandez-Jimenez 2006). The CO_2 uptake in SS(P)_C10 and NS(P)_C10 samples in the proposed temperature range was approximately twice as high as that in PC(P)_C10 sample (see Table 8). It can be inferred from the results that porous concrete fabricated with an AAS paste can be a more effective CO_2 absorber in comparison with that fabricated with an OPC paste.

3.2 Physical Properties of Carbonated Porous Concrete

The measured total void ratios and the targeted void ratios of the porous concretes are listed in Table 9. The target void ratio was calculated based on the P/G ratio. The test results showed that the measured total void ratios of all specimens were much higher than the target void ratios. The fractional excess level between the measured total void ratio and the target void ratio was in the range of 11–31 %. The rough surface and porous internal structure of BA and compaction process for fabrication of the porous concretes may have caused such differences (Singh and Siddique 2014).

Carbonation affected the total void ratios in all the specimens as shown in Table 9. After exposure to accelerated carbonation, the total void ratios of the porous concretes reduced, and the reduction at a 10 % CO_2 concentration was as much as 10 %. In the present study, In spite of the reduction in void ratios after carbonation, the total void ratios of the porous concretes exceeded minimum void ratio of 15 % stated in ACI 522 (American Concrete Institute 2010).

The open and closed void ratios of porous concretes according to the CO_2 concentration are given in Table 10. Most of the voids in the porous concretes consisted of open-voids ranging from 20 to 39 %, while the closed-void was ranged from 5 to 15 %. After the carbonation, the reduction in the closed-void ratios in SS and NS series specimens was greater than that in the open-void ratios. The closed-void ratios were reduced in the range of 1–8 %, while the open-void ratios were reduced in the range of 0–4 %. The residues in the pore solution of the closed-voids can react with CO_2, and the reaction products such as calcium and sodium carbonates may be filled in the closed-voids. Bernal et al. reported that carbonation of AAS pastes mainly occurs in the pore solutions (Bernal et al. 2014). In contrast, the surfaces of the open-voids may be covered with a relatively small amount of solution due to the continuity of the open-voids. Consequently, the reduction of the closed-void ratios in SS and NS series specimens after carbonation was greater than that of open-void ratios.

The reductions in the closed-void ratios of PC2 specimen were relatively lower than that in the SS and NS series specimens. As mentioned above, the porosity of the OPC paste shown in the MIP test result decreased after carbonation, while that of the AAS paste increased. It can be inferred from the results that the reduction in the porosity of the OPC paste interrupted the filling of the closed-voids as carbonation progressed, whereas the formation of carbonated products in the closed-voids of the AAS pastes accelerated (see Table 6).

The test results of compressive strength on porous concretes are shown in Fig. 3. The compressive strength of NS(P), PC(P), and SS(P) pastes in the present study were 23, 45 and 78 MPa, respectively, showing significant difference. The difference in the compressive strength between NS(P) and SS(P) is due that the hydration products in SS(P) is more densified by soluble silicate in waterglass than that in NS(P) (Phoo-ngernkham et al. 2015). However, the compressive strength of NS2_C0, PC2_C0, and SS2_C0 exhibited comparable regardless of the strength of the pastes, when the total void ratios of the porous concretes was similar. Furthermore, when NS series and SS series had comparable total void ratios, the compressive strengths were almost similar. It has been reported in previous studies that the main factor which affects the compressive strength of porous concrete is the total void ratio (Sriravindrarajah et al. 2012; Jang et al. 2015a; Lian et al. 2011; Bhutta et al. 2013).

Table 9 Measured total void ratios and targeted void ratios of porous concretes.

	Exposure condition (CO_2, %)	NS1	NS2	NS3	SS1	SS2	SS3	PC2
V_{target} (%)	–	36	31	26	36	31	26	31
V_{total} (%)	–	40	39	35	46	38	32	37
	5	37	39	29	45	41	33	37
	10	34	33	25	39	36	25	32

Table 10 Open and closed void ratios of porous concretes.

	Exposure condition (CO_2, %)	NS1	NS2	NS3	SS1	SS2	SS3	PC2
V_{open} (%)	–	31	30	20	39	32	24	32
	5	33	35	23	42	37	29	33
	10	29	28	18	36	32	20	28
V_{close} (%)	–	9	9	15	7	6	8	5
	5	4	4	6	3	4	4	5
	10	5	5	7	3	4	5	4

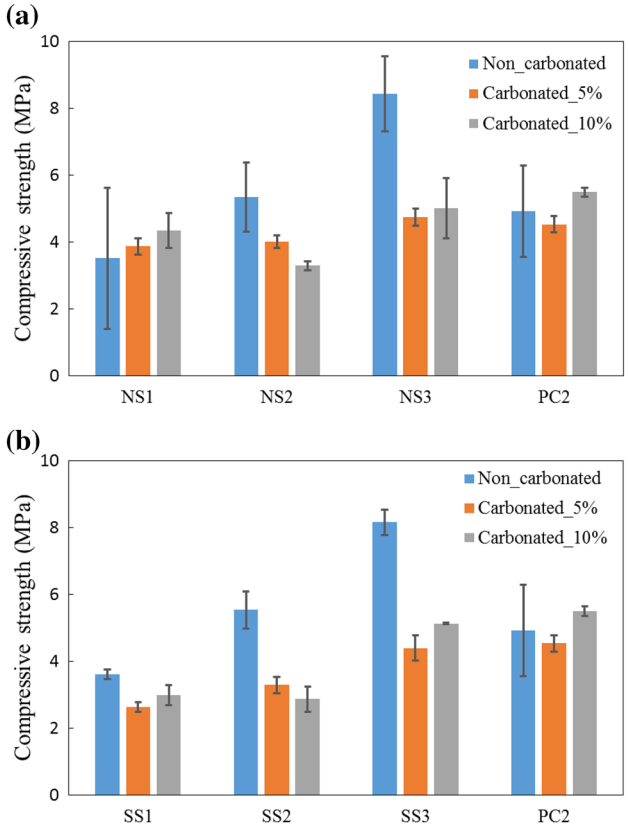

Fig. 3 Compressive strength of porous concretes: **a** fabricated with AAS pastes with NaOH (NS series) and **b** fabricated with AAS pastes with waterglass (SS series).

The compressive strength of the carbonated NS series and SS series decreased compared to non-carbonated specimens, whereas the opposite trend was observed for the PC2 specimen. It can be implied with the results of TG analysis and MIP test that the reduction in compressive strength of NS and SS series after carbonation was responsible for a decrease in the C–S–H phases due to decalcification and an increase in the porosity. However, the reduced compressive strength satisfied the minimum value noted in ACI 522 (2.8 MPa) (American Concrete Institute 2010).

3.3 Heavy Metal Leaching Characteristics of Carbonated Porous Concrete

The test result of an accumulated leaching concentration of heavy metals with exposure sequence in accordance with NSF/ANSI 61-2007a is shown in Fig. 4. The leached concentrations of Cr, Pb and Cd from the OPC-based porous concrete were observed to be higher than those from the AAS-based porous concretes. Bhutta et al. reported that Cr can be evenly distributed in the C–S–H phases of AAS paste, whereas the hydrated calcium aluminate phases in the OPC paste primarily bound Cr ions (Bhutta et al. 2013). It seems that a large amount of Cr in the test was immobilized in NS2 and SS2 specimens, since the C–S–H phases in AAS is a major reaction products. Shi and Fernandez-Jimenez reported that Pb in alkali activated cementitious material can be precipitated as Pb_3SiO_5, which is a highly insoluble silicate (Shi and Fernandez-Jimenez 2006). In the test, it seemed that Pb component in NS2 and SS2 be immobilized by the formation of Pb_3SiO_5.

The leached concentrations of Cr and Pb were not affected by the carbonation. Otherwise, the effect of carbonation on leachability of Cd was differed from that of Cr and Pb. The leached concentration of Cd from PC2_C10 and SS2_C10 specimens was higher than that of non-carbonated PC2_C0 and SS2_C0 specimens. The increased concentration of Cd may be due to a decrease of pH in carbonated specimens (Fleischer et al. 1974; Halim et al. 2004). In previous studies, solubility of Cd increased with the lowering of pH due to carbonation (Fleischer et al. 1974; Halim et al. 2004).

Arsenic is known to be soluble at a wide range of pH levels, creating oxyanions in solutions (Ravikumar and Neithalath 2013). For that reason, the predominant leaching mechanism of As may take place by washing off of leachate from the surface of the porous concretes. However, the leached concentration of As in PC2 specimen was relatively lower than that from the NS2 and SS2 specimens. Vandecasteele et al. reported that As can be reacted with $Ca(OH)_2$ in OPC paste to form the insoluble $Ca_3(AsO_4)$ (Vandecasteele et al. 2002). In contrast, $Ca(OH)_2$ is not present in the AAS matrix (Shi and Fernandez-Jimenez 2006). Therefore, it can be inferred that As in PC2 specimen was immobilized

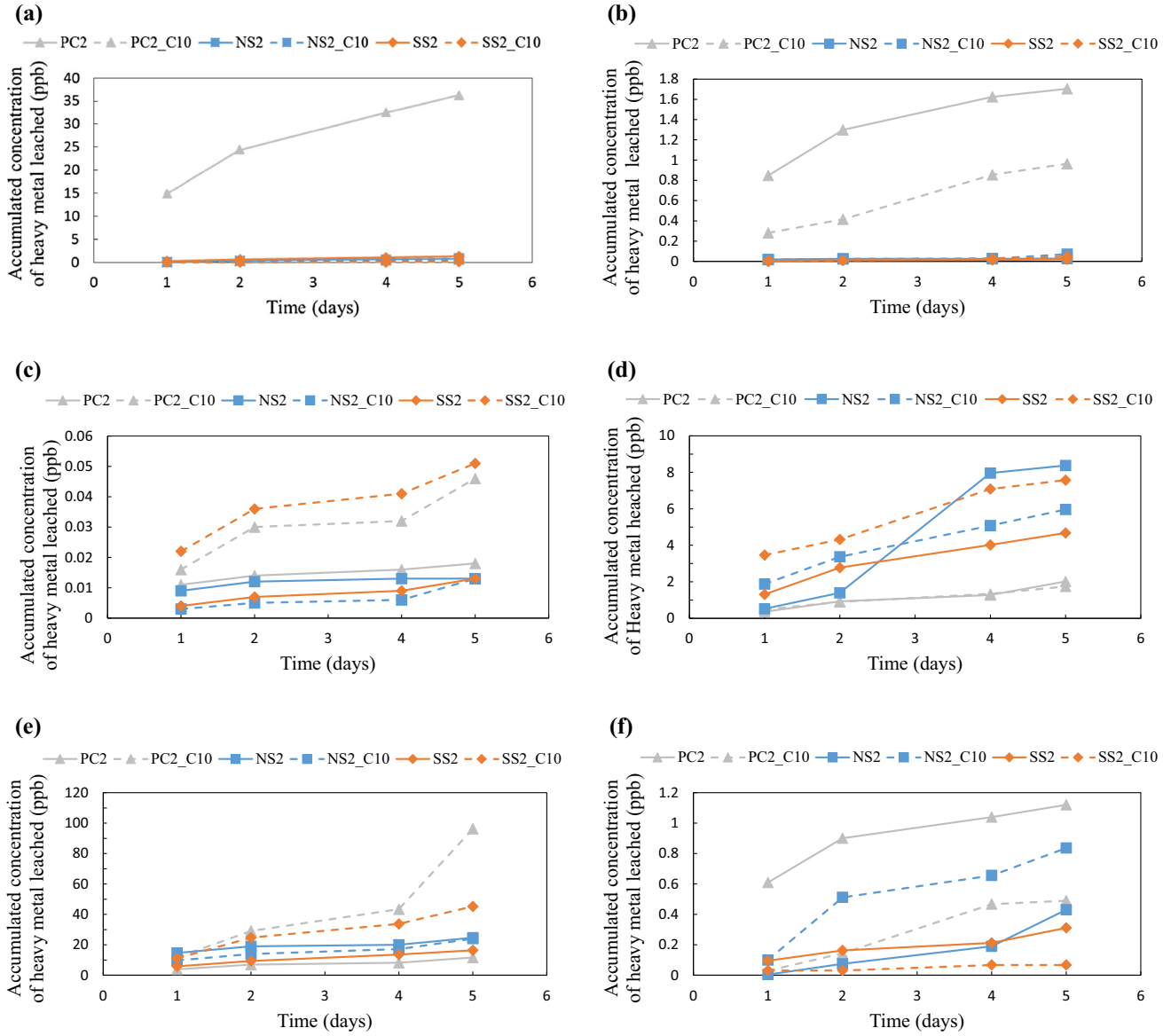

Fig. 4 Accumulated concentration of heavy metals leached from porous concretes: **a** chromium, **b** lead, **c** cadmium, **d** arsenic, **e** copper and **f** mercury.

Table 11 Single time-point concentration of the leached heavy metal according to NSF/ANSI 61-2007a, the drinking water regulatory level criteria (MCL/MAC) and the single-product allowable concentration (SPAC) (NSF International standard/American National Standard, NSF/ANSI 61- 2007a 2007).

(mg/L)	Cr	Cu	As	Pb	Cd	Hg
PC2_C0	0.003747	0.003361	0.00074	0.00008	2E−0.6	0.00008
NS2_C0	0.000168	0.004682	0.00041	3E–06	ND[a]	0.00024
SS2_C0	0.000248	0.002800	0.00066	6E–06	4E−06	0.00009
PC2_C10	0.00011	0.05289	0.00041	0.00015	0.00001	0.00002
NS2_C10	0.00011	0.00681	0.00088	0.00004	7E−06	0.00018
SS2_C10	0.00005	0.01154	0.00049	0.00002	0.00001	ND
MCL/MAC	0.1	1.3	0.01	0.015	0.005	0.002
SPAC	0.01	0.13	0.001	0.0015	0.0005	0.0002

[a] ND: Non detected.

by the formation of $Ca_3(AsO_4)$, whereas As in NS2 and SS2 specimens was washing off from the surface of them.

The leached concentrations of Cu from PC2_C0 specimen were lower than those from NS2_C0 and SS2_C0 specimens, as shown in Fig. 4e. In addition, the leached Cu concentrations in all specimens increased after carbonation. The increased Cu concentrations may be caused by a decrease of pH due to carbonation. Bochenczyk reported that solubility of Cu can increase by lowering of pH due to carbonation (Zhang et al. 2007; Bochenczyk 2010). That is, the solubility of Cu in all carbonated porous concretes may increase, since the carbonation can be lower the pH of all specimens (Puertas et al. 2006; Bernal et al. 2014). The immobilization of Hg in PC2 specimen was not effective in comparison with that in the NS2 and SS2 specimens, as shown in Fig. 4f. Qian et al. reported that the immobilization of Hg in AAS matrix is highly effective, since physical encapsulation and chemical fixation are contributed to immobilization of Hg (Bakharev et al. 2001; Qian et al. 2003c). Thus, it seems that the two mechanisms in the test lowered leached concentration of Hg from NS2 and SS2 specimens.

Lastly, the test results of the single-point concentration of the leached heavy metals, the drinking water regulatory level criteria (MCL/MAC), and the single-product allowable concentration (SPAC) are shown in Table 11. The concentrations of the leached heavy metals from all the specimens, except for Hg in NS2, satisfied the criteria specified in MCL/MAC and SPAC. The exceeding amount of Hg in NS2 was not significant.

4. Concluding Remarks

In the present study, a porous concrete with alkali activated slag and coal bottom ash was developed and the effect of carbonation on physical property, microstructural characteristic, and heavy metal leaching behavior of the porous concrete were investigated. Independent variables, such as the type of the alkali activator and binder, the amount of paste, and CO_2 concentration, were considered. The main conclusions can be summarized below:

(1) Void ratio and compressive strength of AAS-based porous concretes were reduced by carbonation, and the measured void ratio and compressive strength of the carbonated porous concretes in the test exceeded the minimum level stated in ACI 522 for general porous concrete.

(2) Reduction of void ratio in carbonated AAS-based porous concrete mainly occurred in closed-voids. Reduction of compressive strength in the carbonated porous concrete may be attributed by an increase in porosity and decomposition of C–S–H phases.

(3) An amended temperature range in TG/DTA analysis was proposed to more accurately evaluate CO_2 uptake in AAS pastes, considering sodium and calcium carbonates. The CO_2 uptake of AAS pastes in the proposed temperature range was approximately twice as high as that in OPC paste.

(4) The Immobilization of chromium, lead, cadmium and mercury in the AAS-based porous concretes was more effective in comparison with that in the OPC-based porous concrete, and carbonation of the AAS based-porous concretes could cause an increase in the leached concentration of cadmium and copper. However, the leached concentrations of heavy metals in porous concretes utilizing AAS and BA in the test were all below the SPAC and MCL/MAC criteria as described in the NSF/ANSI 61-2007a.

Acknowledgments

This research was supported by a grant from the Energy Technology Development Program (grant No. 2013T100100021) funded by the Ministry of Trade Industrial and Energy of the Korea government, and by Saudi Aramco-KAIST CO2 Management Center.

Open Access

References

American Concrete Institute, ACI 522R-10. Report on pervious concrete. ACI Committee 522 2010.

American Society for Testing and Materials, ASTM C39. (2012). *Standard test method for compressive strength of cylindrical concrete specimens*. West Conshohocken, PA: ASTM International.

Bakharev, T., Sanjayan, J. G., & Cheng, Y.-B. (2001). Resistance of alkali-activated slag concrete to carbonation. *Cement and Concrete Research, 31*, 1277–1283.

Bernal, S. A., Nicolas, R., Provis, J. L., De Gutierrez, R. M., & van Deventer, J. S. (2014). Natural carbonation of aged alkali-activated slag concretes. *Materials and Structures, 47*, 693–707.

Bertos, M. F., Simons, S. J. R., Hills, C. D., & Carey, P. J. (2004). A review of accelerated carbonation technology in the treatment of cement-based materials and sequestration of CO_2. *Journal of Hazardous Materials, 112*(2), 193–205.

Bhutta, M. A. R., Hasanah, N., Farhayu, N., Hussin, M. W., Tahir, M. B. M., & Mirza, J. (2013). Properties of porous

concrete from waste crushed concrete (recycled aggregate). *Construction and Building Materials, 47*, 1243–1248.

Bhutta, M. A. R., Tsuruta, K., & Mirza, J. (2012). Evaluation of high-performance porous concrete properties. *Construction and Building Materials, 31*, 67–73.

Bochenczyk, A. U. (2010). Mineral sequestration of CO2 in suspensions containing mixtures of fly ashes and desulphurization waste. *Gosposarka Surowcami Mineralnymi, 26*, 109–118.

Chi, M.C., Chang, J.J., & Huang, R. (2012). Strength and drying shrinkage of alkali-activated slag paste and mortar. *Advances in Civil Engineering,* 2012.

Deja, J. (2002). Immobilization of Cr^{6+}, $Cd^{2+,}$ Zn^{2+} and Pb^{2+} in alkali-activated slag binders. *Cement and Concrete Research, 32*, 1971–1979.

Dermatas, D., & Meng, X. (2003). Utilization of fly ash for stabilization/solidification of heavy metal contaminated soil. *Engineering Geology, 70*, 337–394.

Edwards, H. G., Currie, K. J., Ali, H. R., Villar, S. E. J., David, A. R., & Denton, J. (2007). Raman spectroscopy of natron: shedding light on ancient Egyptian mummification. *Analytical and Bioanalytical Chemistry, 388*(3), 683–689.

Ekmekyapar, A., Ersahan, H., & Yapici, S. (1996). Non-isothermal decomposition kinetics of trona. *Industrial and Engineering Chemistry Research, 35*, 258–262.

Eloneva, S., Teir, S., Salminen, J., Fogelholm, C. J., & Zevenhoven, R. (2008). Fixation of CO2 by carbonating calcium derived from blast furnace slag. *Energy, 33*, 1461–1467.

Environment, Health and Safety Online. (2008). The EPA TCLP: Toxicity characteristic leaching procedure and characteristic wastes (D-codes). Environment, Health and Safety Online.

Fleischer, M., Sarofim, A. F., Fassett, D. W., Hammond, P., Shacklette, H. T., Nisbet, I. C., & Epstein, S. (1974). Environmental impact of cadmium: a review by the Panel on Hazardous Trace Substances. *Environmental Health Perspectives, 7*, 253.

Guo, Q., Qu, J., Qi, T., Wei, G., & Han, B. (2011). Activation pretreatment of limonitic laterite ores by alkali-roasting method using sodium carbonate. *Minerals Engineering, 24*, 825–832.

Halim, C. E., Acott, J. A., Natawardaya, H., Amal, R., Beydoun, D., & Low, G. (2004). Comparison between acetic acid and landfill leachates for the leaching of Pb(II), Cd(II), As(V), and Cr(VI) from cementitious wastes. *Environmental Science and Technology, 38*, 3977–3983.

Jang, J. G., Ahn, Y. B., Souri, H., & Lee, H. K. (2015a). A novel eco-friendly porous concrete fabricated with coal ash and geopolymeric binder: Heavy metal leaching characteristics and compressive strength. *Construction and Building Materials, 79*, 173–181.

Jang, J. G., Kim, H. J., Park, S. M., & Lee, H. K. (2015b). The influence of sodium hydrogen carbonate on the hydration of cement. *Construction and Building Materials, 94*, 746–749.

Japanese Standard Association, JIS A 1104. (2006). Methods of test for bulk density of aggregates and solid content in aggregates. JSA

Kar, A., Ray, I., Halabe, U. B., Unnikrishnan, A., & Dawson-Andoh, B. (2014). Characterizations and quantitative estimation of alkali-activated binder paste from microstructures. *International Journal of Concrete Structures and Materials, 8*, 213–228.

Kim, H. K., Ha, K. A., Jang, J. G., & Lee, H. K. (2014a). Mechanical and chemical characteristics of bottom ash aggregates cold-bonded with fly ash. *Journal of Korean Ceramic Society, 51*, 57–63.

Kim, H. K., Jang, J. G., Choi, Y. C., & Lee, H. K. (2014b). Improved chloride resistance of high-strength concrete amended with coal bottom ash for internal curing. *Construction and Building Materials, 71*, 334–343.

Kim, M. S., Jun, Y., Lee, C., & Oh, J. E. (2013). Use of CaO as an activator for producing a price-competitive non-cement structural binder using ground granulated blast furnace slag. *Cement and Concrete Research, 54*, 208–214.

Kim, H. K., & Lee, H. K. (2010). Influence of cement flow and aggregate type on the mechanical and acoustic characteristics of porous concrete. *Applied Acoustics, 71*, 607–615.

Kuo, W. T., Liu, C. C., & Su, D. S. (2013). Use of washed municipal solid waste incinerator bottom ash in pervious concrete. *Cement & Concrete Composites, 37*, 328–335.

Li, X. D., Poon, C. S., Sun, H., Lo, I. M. C., & Kirk, D. W. (2012). Heavy metal speciation and leaching behaviors in cement based solidified/stabilized waste materials. *Journal of Hazardous Materials, 82*(3), 215–230.

Lian, C., Zhuge, Y., & Beecham, S. (2011). The relationship between porosity and strength of porous concrete. *Construction and Building Materials, 25*, 4292–4298.

NSF International standard/American National Standard, NSF/ANSI 61-2007a. (2007). *Drinking water system components—health effects*. Oxfordshire: NSF International.

Park, S. B., & Tia, M. (2004). An experimental study on the water purification properties of porous concrete. *Cement and Concrete Research, 34*, 177–184.

Perera, D. S., Aly, Z., Vance, E. R., & Mizumo, M. (2005). Immobilization of Pb in a geopolymer matrix. *Journal of the American Ceramic Society, 88*, 2586–2588.

Phoo-ngernkham, T., Maegawa, A., Mishima, N., Hatanaka, S., & Chindaprasirt, P. (2015). Effects of sodium hydroxide and sodium silicate solutions on compressive and shear bond strengths of FA-GBFS geopolymer. *Construction and Building Materials, 91*, 1–8.

Puertas, F., Palacious, M., & Vazquez, T. (2006). Carbonation process of alkali-activated slag mortars. *Journal of Materials Science, 41*, 3071–3082.

Qian, G., Sun, D. D., & Tay, J. H. (2003a). Immobilization of mercury and zinc in an alkali-activated slag matrix. *Journal of Hazardous Materials, 101*(2), 65–77.

Qian, G., Sun, D. D., & Tay, J. H. (2003b). Characterization of mercury- and zinc-doped alkali-activated slag matrix Part II. *Zinc. Cement and Concrete Research, 33*, 1257–1262.

Qian, G., Sun, D. D., & Tay, J. H. (2003c). Characterization of mercury- and zinc-doped alkali-activated slag matrix Part I. *Mercury. Cement and Concrete Research, 33*, 1251–1256.

Ravikumar, D., & Neithalath, N. (2013). Electrically induced chloride ion transport in alkali activated slag concretes and

the influence of microstructure. *Cement and Concrete Research, 47*, 31–42.

Shi, C., & Fernandez-Jimenez, A. (2006). Stabilization/solidification of hazardous and radioactive wastes with alkali-activated cements. *Journal of Hazardous Materials, 137*(3), 1656–1663.

Singh, M., & Siddique, R. (2014). Strength properties and micro-structural properties of concrete containing coal bottom ash as partial replacement of fine aggregate. *Construction and Building Materials, 50*, 246–256.

Song, S., & Jennings, H. M. (1999). Pore solution chemistry of alkali-activated ground granulated blast-furnace slag. *Cement and Concrete Research, 29*, 159–170.

Sriravindrarajah, R., Wang, N. D. H., & Ervin, L. J. W. (2012). Mix design for pervious recycled aggregate concrete. *International Journal of Concrete Structures and Materials, 6*(4), 239–246.

Vandecasteele, C., Dutre, V., Geysen, D., & Wauters, G. (2002). Solidification/stabilization of arsenic bearing fly ash from the metallurgical industry. Immobilization mechanism of arsenic. *Waste Management, 22*(2), 143–146.

Wang, S. D., & Scrivener, K. L. (1995). Hydration products of alkali activated slag cement. *Cement and Concrete Research, 25*, 561–571.

Ylmén, R., & Jäglid, U. (2013). Carbonation of Portland cement studied by diffuse reflection fourier transform infrared spectroscopy. *International Journal of Concrete Structures and Materials, 7*, 119–125.

Zhang, J., Provis, J. L., Feng, D., & van Deventer, J. S. J. (2008). Geopolymers for immobilization of Cr^{6+}, Cd^{2+}, and Pb^{2+}. *Journal of Hazardous Materials, 157*, 587–598.

Zhang, Y., Sun, W., Chen, Q., & Chen, L. (2007). Synthesis and heavy metal immobilization behaviors of slag based geopolymer. *Journal of Hazardous Materials, 143*, 206–213.